




RESEARCH ARTICLE | JANUARY 03 2023

## Hybrid magnetization dynamics in $\text{Cu}_2\text{OSeO}_3/\text{NiFe}$ heterostructures

Carolina Lüthi ; Luis Flacke ; Aisha Aqeel ; Akashdeep Kamra ; Rudolf Gross ; Christian Back ; Mathias Weiler  

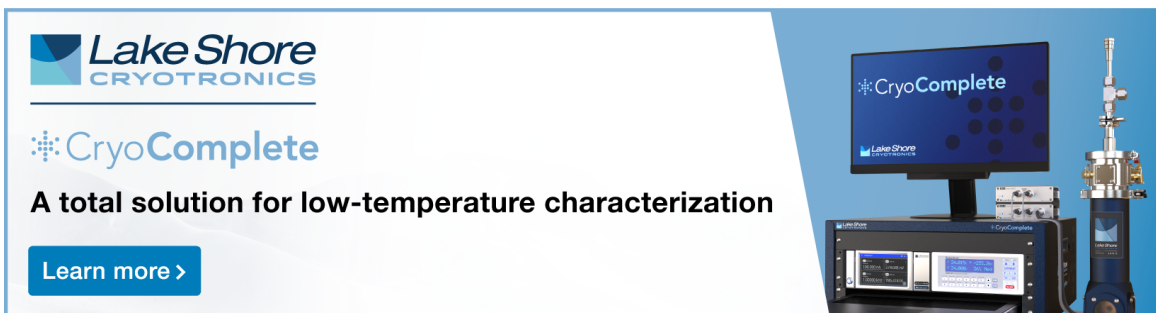
 Check for updates


*Appl. Phys. Lett.* 122, 012401 (2023)

<https://doi.org/10.1063/5.0128733>



CrossMark



  
**CryoComplete**  
A total solution for low-temperature characterization  
[Learn more >](#)

The advertisement features a photograph of the CryoComplete system, which includes a computer monitor displaying the software interface, a control unit, and a cryogenic probe.

# Hybrid magnetization dynamics in $\text{Cu}_2\text{OSeO}_3/\text{NiFe}$ heterostructures

Cite as: Appl. Phys. Lett. **122**, 012401 (2023); doi: [10.1063/5.0128733](https://doi.org/10.1063/5.0128733)

Submitted: 30 September 2022 · Accepted: 20 December 2022 ·

Published Online: 3 January 2023



View Online



Export Citation



CrossMark

Carolina Lüthi,<sup>1,2</sup>  Luis Flacke,<sup>1,2</sup>  Aisha Aqeel,<sup>2,3</sup>  Akashdeep Kamra,<sup>4</sup>  Rudolf Gross,<sup>1,2,3</sup>   
Christian Back,<sup>2,3</sup>  and Mathias Weiler<sup>1,2,5,a)</sup> 

## AFFILIATIONS

<sup>1</sup>Walther-Meißner-Institut, Bayerische Akademie der Wissenschaften, Garching, Germany

<sup>2</sup>Physics Department, Technical University of Munich, Garching, Germany

<sup>3</sup>Munich Center for Quantum Science and Technology (MCQST), Munich, Germany

<sup>4</sup>Condensed Matter Physics Center (IFIMAC) and Departamento de Física Teórica de la Materia Condensada, Universidad Autónoma de Madrid, Madrid, Spain

<sup>5</sup>Fachbereich Physik and Landesforschungszentrum OPTIMAS, Technical University of Kaiserslautern, Kaiserslautern, Germany

<sup>a)</sup>Author to whom correspondence should be addressed: [weiler@physik.uni-kl.de](mailto:weiler@physik.uni-kl.de)

## ABSTRACT

We investigate the coupled magnetization dynamics in heterostructures of a single crystal of the chiral magnet  $\text{Cu}_2\text{OSeO}_3$  (CSO) and a polycrystalline ferromagnet NiFe (Py) thin film using broadband ferromagnetic resonance (FMR) at cryogenic temperatures. We observe the excitation of a hybrid mode (HM) below the helimagnetic transition temperature of CSO. This HM is attributed to the spin dynamics at the CSO/Py interface. We study the HM by measuring its resonance frequencies for in plane rotations of the external magnetic field. We find that the HM exhibits dominantly fourfold anisotropy in contrast to the FMR of CSO and Py.

© 2023 Author(s). All article content, except where otherwise noted, is licensed under a Creative Commons Attribution (CC BY) license (<http://creativecommons.org/licenses/by/4.0/>). <https://doi.org/10.1063/5.0128733>

Chiral magnets exhibit non-collinear spin structures, such as spin helices and magnetic skyrmions, below their critical temperature  $T_c$  and critical field  $H_{c2}$ .<sup>1</sup> Skyrmions are topologically protected non-coplanar magnetization configurations that can behave as particle-like objects. Furthermore, they are small yet stable, making them suitable to become the carriers of information in future devices.<sup>2–12</sup> The non-collinear spin structure of chiral magnets gives rise to intriguing magnetization dynamics, in particular in their skyrmion lattice phase.<sup>13</sup> The recently discovered low-temperature skyrmion phase<sup>14</sup> leads to additional striking spin dynamical signatures<sup>15</sup> in the low-damping<sup>16</sup> chiral magnet  $\text{Cu}_2\text{OSeO}_3$  (CSO). The periodicity of the magnetic lattice leads to naturally formed magnonic crystals<sup>17</sup> and the skyrmion eigenmodes can be coupled to photonic resonators with high cooperativity.<sup>18</sup> The chiral properties of skyrmions give rise to non-reciprocal spin-wave dynamics.<sup>19</sup> Thus, the emerging field of spin dynamics of chiral magnets has already revealed important fundamental insight with perspectives for practical applications.

In topologically trivial magnets, the now well studied coupling between multiple magnetic layers<sup>20–26</sup> resulted in the discovery of some of the most technologically relevant effects, such as tunneling

magnetoresistance<sup>27</sup> or giant magnetoresistance.<sup>28,29</sup> Heterostructures of topologically trivial magnets can exhibit coupled spin dynamics that can lead to, e.g., excitation of nanoscale spin waves.<sup>30</sup> Much less is known about spin dynamics in heterostructures of collinear and chiral magnets. The coupling between distinct order parameters across interfaces has explained important phenomena, such as proximity effects, exchange bias, or exchange spring-induced hard magnets.<sup>31</sup> However, the studies of excitations in chiral magnets are so far limited to a single magnetically ordered constituent.<sup>32</sup> Even though the formation of novel topological order at the chiral magnet/ferromagnet interface was predicted by theory, it has not yet been observed in experiment.<sup>33</sup>

In this work, we investigate the hybrid magnetization dynamics of heterostructures of thin film metallic ferromagnets and bulk chiral magnets, in this case the ferrimagnetic insulator  $\text{Cu}_2\text{OSeO}_3$  (CSO). To study the magnetization dynamics of the chiral magnet/ferromagnet heterostructures in the GHz frequency regime, we use broadband ferromagnetic resonance (FMR) spectroscopy. We experimentally determine and phenomenologically model the resonance frequencies in such heterostructures. Thereby, we find that a hybrid mode of the chiral magnet/ferromagnet heterostructure is excited, which we attribute

to the spin dynamics at the interface of the two magnetic layers. We investigate a CSO/Ni<sub>80</sub>Fe<sub>20</sub> (CSO/Py) sample, where the Py thin film has a thickness of 40 nm. The CSO crystal is (111)-oriented and cut to a cuboid shape with dimensions  $L_x = 2.5$  mm,  $L_y = 1.5$  mm, and  $L_z = 0.8$  mm. It was grown by a chemical vapor transport method<sup>35</sup> (for details on the crystal orientation of the CSO and the sample preparation, see [supplementary material S1](#) and [S2](#)). We place the CSO/Py hybrid on top of a coplanar waveguide (CPW) with a center conductor width of  $w = 127$   $\mu\text{m}$  as shown in [Fig. 1\(a\)](#). The CPW is connected to two ports P1 and P2 of a vector network analyzer (VNA), which measures the change of transmission from P1 to P2 defined as the complex transmission parameter  $S_{21}$  as a function of frequency  $f$  and external magnetic field  $\mu_0 H$  at a fixed microwave power of 1 mW (0 dBm). We then place the CPW/CSO/Py assembly into the variable temperature insert of a superconducting 3D-vector magnet. By applying a static external magnetic field  $\mu_0 \mathbf{H}$  in the plane of the Py thin film and setting the temperature to 5 K, we can access the helical (H), conical (C), and ferrimagnetic (F) phases of the CSO<sup>17</sup> as schematically depicted in [Fig. 1\(b\)](#). See the [supplementary material S3](#) for an illustration of the phases of CSO in dependence of the frequency and field.

As a reference measurement, we first place the CSO/Py hybrid sample on the CPW with the Py facing away from the CPW. Due to the large thickness of the CSO layer, the oscillating magnetic field generated by the CPW does not reach the Py layer. In this way, we only excite the magnetization in CSO itself with no influence of the Py layer. We apply a fixed external magnetic field  $\mu_0 H = 120$  mT along the x-axis ( $\phi_H = 0^\circ$ ) at 5 K, as illustrated schematically in the top panel of [Fig. 2\(a\)](#). For this temperature and external magnetic field strength, the CSO magnetization is in the field polarized phase. To correct for the microwave background of the complex transmission parameter  $S_{21}$ , we use the derivative divide method<sup>36</sup> to obtain the field derivative of the complex transmission parameter  $\frac{\partial S_{21}}{\partial H}$  divided by  $S_{21}$ . On the bottom panel of [Fig. 2\(a\)](#),  $\text{Re}(\partial_D S_{21} / \partial H)$  for the CPW/CSO/Py assembly at 5 K is shown as a function of the frequency  $f$ . In the gray marked frequency range, several resonances appear. These are attributed to the excitation of magnetostatic modes of the cuboid-shaped CSO crystal. In the frequency range  $7 \text{ GHz} < f < 12 \text{ GHz}$ , no

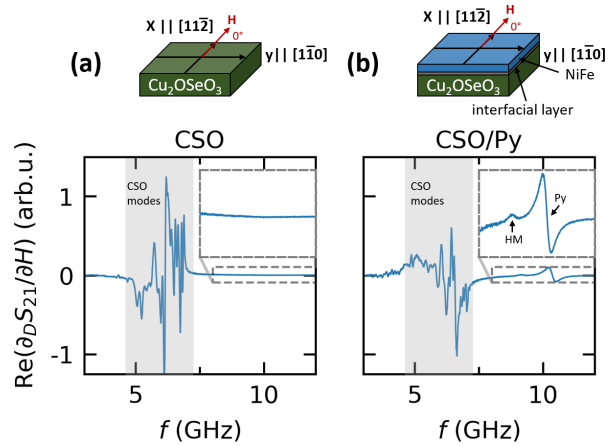


**FIG. 2.** Measured broadband ferromagnetic resonance spectrum of the CSO/Py sample at 5 K as a function of the frequency  $f$ . The fixed external magnetic field  $\mu_0 H = 120$  mT is applied along the x-axis ( $\phi_H = 0^\circ$ ) as indicated in the sample sketches. (a) The CSO crystal faces the CPW. Thus, only ferrimagnetic CSO modes appear (gray marked frequency range). (b) The Py thin film faces the CPW. In addition to the CSO modes, the Py FMR mode appears at high frequencies as well as a hybrid mode (HM) at medium frequencies (inset). This HM is attributed to the spin dynamics at the interface of the CSO/Py sample, indicated as an interfacial layer in the sample sketch.

additional modes are observed (inset). After determining the response of the isolated CSO magnetization dynamics, we place the CSO/Py hybrid on the CPW with the Py facing the CPW and again apply a fixed magnetic field  $\mu_0 H = 120$  mT along the x-axis as schematically shown in the top panel of [Fig. 2\(b\)](#). Now, the field generated by the CPW interacts with the Py layer as well as the CSO as the Py layer is a thin film. In the bottom panel of [Fig. 2\(b\)](#),  $\text{Re}(\partial_D S_{21} / \partial H)$  at 5 K is shown for the CPW/Py/CSO assembly as a function of the frequency  $f$ . In addition to the resonance lines of CSO (gray marked frequency range), the Py FMR line also appears close to 10 GHz as expected. The change in the CSO mode spectrum is attributed to the presence of the metallic film and concomitant shielding of the microwave field in the bulk of CSO. Furthermore, we observe an additional medium frequency mode, which is shifted by about 1 GHz to lower frequencies than the Py FMR mode. This hybrid mode (HM) is also observed in the CSO/Py hybrid in the conical phase of CSO (see [Fig. S2](#) in the [supplementary material](#)). For the dependence of the HM on the magnitude of the external magnetic field, see [supplementary material S3](#). We attribute the appearance of this additional mode to the spin dynamics at the CSO/Py interface. Thus, in a simplified macrospin picture, we may treat our bilayer as a trilayer with a new interfacial layer inheriting properties from both sides. The HM is then modeled as a result of macrospin dynamics of the interlayer as discussed in the following.

To investigate the dependence of the HM on the direction of the external magnetic field, we apply a field with a fixed magnitude of  $\mu_0 H = 120$  mT and rotate the field direction by  $360^\circ$  in the Py film plane. For a quantitative analysis of the HM, we simultaneously fit the Py FMR peak and the HM peak in the frequency domain of the transmission parameter  $S_{21}$  for each fixed external field direction (for detailed information on the fit model, see [supplementary material S4](#)). In [Fig. 3](#), three exemplary fits of the frequency spectrum are shown for

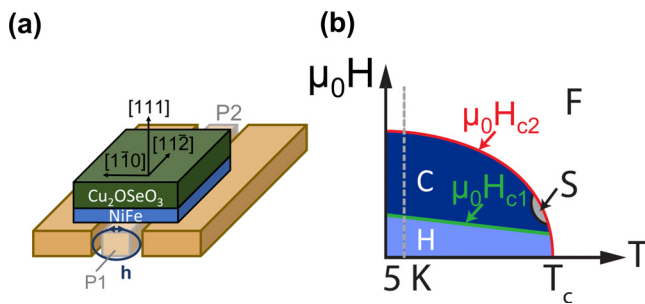


**FIG. 1.** (a) Experimental setup: the (111)-oriented  $\text{Cu}_2\text{OSeO}_3/\text{NiFe}$  heterostructure is placed on the CPW, which generates a magnetic field ( $h$ ) within the sample due to the application of an ac flowing from port 1 (P1) to port 2 (P2) of the center conductor. (b) Schematic phase diagram of the  $\text{Cu}_2\text{OSeO}_3$  crystal defining the helimagnetic transition temperature  $T_c = 58.2$  K (Ref. 34) as well as the critical fields  $\mu_0 H_{c1}$  and  $\mu_0 H_{c2}$  (H: helical state, C: conical state, S: skyrmionic state, F: ferrimagnetic state). The vertical dashed line indicates the phases of the CSO at 5 K in dependence of the external field.

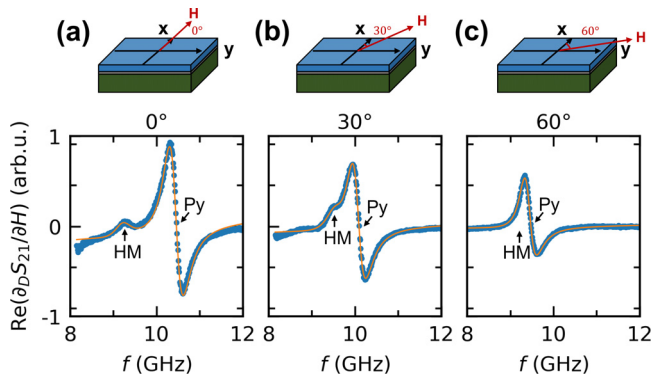


**FIG. 3.** Fits of the frequency spectrum for a fixed magnitude of the external field  $\mu_0 H = 120$  mT at 5 K. The magnetic field direction is rotated in the Py thin film plane and defined by the angle  $\phi_H$  with respect to the x-axis as indicated in the sketches of the sample. The blue dots correspond to the measurement data and the orange line to the fit. (a)  $\phi_H = 0^\circ$ . The peak of the HM at 9.2 GHz and the Py FMR peak-dip at 10.4 GHz are clearly separable. (b)  $\phi_H = 30^\circ$ . The two resonance frequencies of the Py mode and the HM are less separated. (c)  $\phi_H = 60^\circ$ . The two resonance frequencies of the Py mode and the HM are not separable anymore.

a fixed magnitude of the field  $\mu_0 H = 120$  mT and for different directions under which it was applied. In Fig. 3(a), the external field is applied in the Py thin film plane along the x-axis as schematically depicted at the top of Fig. 3(a). We find the peak of the hybrid mode at 9.2 GHz, which has small amplitude compared to the Py FMR peak-dip at 10.4 GHz. In Fig. 3(b), we show the fit result for the field applied under an angle  $\phi_H = 30^\circ$  with respect to the x-axis as depicted at the top of Fig. 3(b). Now, the two resonance frequencies of the Py mode and the HM are less separated than in Fig. 3(a), as the hybrid mode moved to higher frequencies and the Py mode to lower frequencies. In Fig. 3(c), the field is applied under an angle  $\phi_H = 60^\circ$ . The two resonance frequencies of the Py mode and the HM are not separable anymore as the HM resonance frequency is presumably superimposed on the Py resonance frequency. Furthermore, the amplitude of the FMR signal decreases in Figs. 3(b) and 3(c). As the applied field shifts away from the x-axis, so does the equilibrium magnetization. As a result, the CPW oscillating field component transverse to the static magnetization also diminishes. This results in a reduction of the recorded FMR signal amplitude.

To better understand the behavior of the spin dynamics in the sample in dependence of the external magnetic field and temperature, we fit the resonance frequencies of each layer for a full rotation of the external field applied in the Py thin film plane, and we evaluate the dependence of the HM resonance frequency on temperature by fitting its resonance frequency for a fixed field direction at different temperatures. In Fig. 4(a), the fitted resonance frequencies at 5 K of the Py FMR mode (blue dots), the CSO modes (green shading indicates the frequency range over which the CSO magnetostatic modes are observed), and the hybrid mode (orange dots) are plotted against the angle  $\phi_H$ . In the fit model, we only consider the CSO mode with the strongest amplitude (green dots). Furthermore, for  $\phi_H \simeq 90^\circ$  we are not able to fit the HM, as it either vanishes or merges with the Py FMR mode. Due to the demagnetization field in the CSO crystal, the CSO resonance frequencies show a cosine like dependence on the angle

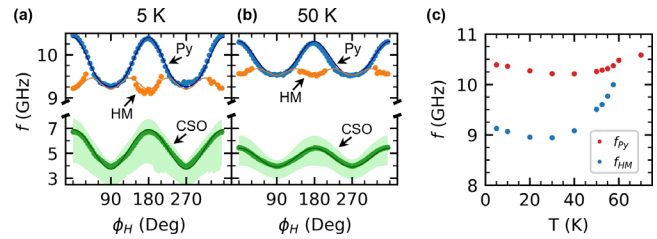


**FIG. 4.** Dependence of the Py (blue dots), CSO (green dots), and HM (orange dots) resonance frequencies on the external magnetic field direction for a  $360^\circ$  rotation in the Py thin film plane and a fixed magnitude  $\mu_0 H = 120$  mT at 5 K (a) and 50 K (b). The green shaded range around the CSO resonance frequencies indicates the frequency distribution of the magnetostatic CSO modes. The fit errors are smaller than the symbol size. The solid lines show the simulation result according to Eq. (1) of the Py (blue line), CSO (green line), and HM (orange line) resonance frequencies which are in good agreement with the measurement data. (c) Fit result of the Py (red dots) and HM (blue dots) resonance frequencies in dependence of the temperature with fixed external field  $\mu_0 H = 120$  mT applied along the x-axis ( $\phi_H = 0^\circ$ ). Above the critical temperature  $T_c = 58.2$  K of the CSO, the HM mode vanishes.

under which the external field is applied. Furthermore, we observe an uniaxial anisotropy in the Py resonance frequencies. This uniaxial anisotropy is strongest for 5 K and weakens for increasing temperatures [see Fig. 4(b) and supplementary material S6]. Additionally, a broadening of the Py resonance minima and a narrowing of the respective peaks is observed. The HM shows a striking feature with its angle dependence being inverted with respect to the CSO and Py modes. Its presence and frequency difference with respect to the Py mode at  $\phi_H = 0^\circ$  vanishes when surpassing the CSO ordering temperature as shown in Fig. 4(c).

The angle and temperature dependence of the observed modes reveals a complex interaction within the heterostructure. In the following, we critically analyze various mechanisms that could potentially underlie the observed HM.

First, we start by noting the effect of CSO on the system. By increasing the temperature, a reduced uniaxial anisotropy not only of the CSO but also of the Py and HM mode becomes evident [see Figs. 4(a) and 4(b) and supplementary material S6]. This reduction agrees with a decreased spin ordering in CSO at higher temperatures, such that the effect of magnetic stray field of the bulk CSO crystal on the Py layer can be assumed to be the dominant effect seen by the uniaxial anisotropy in the Py mode (see calculation of the anisotropy field according to Ref. 37 in the supplementary material S6).

It also supports our inference that CSO plays the main role in determining the frequency of the HM. In the following, we argue that the HM is indeed the result of a coupling of the multilayer system. Figure 4(c) visualizes the dependence of the Py and the HM resonance frequencies on temperature where the external field has a magnitude of 120 mT and is applied under an angle  $\phi_H = 0^\circ$ . With increasing temperature the HM mode approaches the Py mode until it vanishes above 58 K. Thus, above the critical temperature of CSO, the coupling of the CSO and Py dynamics vanishes and the HM cannot be excited any more. This demonstrates that the existence of the HM is a direct consequence of the magnetic ordering of CSO. We may, thus, exclude non-uniformity of the Py layer as its origin.

Assuming exchange interaction and spin torques at the interface similar to in Ref. 30 and including such terms in the Landau-Lifshitz-Gilbert

(LLG) equation would result in four solutions for resonance frequencies. Namely, the uncoupled CSO and Py layer as well as two coupled modes. It might be possible that the second coupled mode is hidden in the series of magnetostatic modes of the CSO. However, in this case, the solutions for the hybrid modes would only lead to a constant shift of the HM frequencies compared to the Py resonance frequencies without an angle dependent gap between the Py and the HM resonance frequencies. Nonetheless, if the exchange interaction was to be anisotropic, a reason for which is not evident to us, the additional degree of freedom could result in the observed symmetry of the HM.

CSO is known for its intrinsic inversion symmetry breaking and the existence of Dzyaloshinskii–Moryia interaction (DMI). As a result, the FMR mode at  $k = 0$  is no longer the lowest frequency mode. The DMI gives rise to a linear-in- $k$  contribution that causes further lowering of frequency for a finite- $k$  spin wave mode.<sup>38</sup> Such a finite- $k$  mode does not experience the same shape anisotropy, parameterized by the demagnetization tensor components, as the FMR modes.<sup>39</sup> Hence, it makes sense for the HM mode to bear a different angular dependence than the Py and CSO FMR modes dominated by the shape anisotropy. Furthermore, a lowering of the frequency by the DMI term<sup>38</sup> is consistent with the HM mode appearing below the Py FMR modes. It is, however, not clear to us why the finite- $k$  mode at the lowest frequency should be excited in this bilayer and act as an additional mode, although it cannot be ruled out. The observed angle-dependence of the HM is still not obvious in that case and may require considering the pinning caused by the DMI at the edges.<sup>38</sup>

Another observation that makes a clear interpretation difficult is the broadening/narrowing of the Py resonance minima/maxima. Such a behavior is usually seen in material systems with a cubic, i.e., fourfold symmetry superimposed with the previously described uniaxial anisotropy.<sup>40</sup> This contradicts the threefold symmetry that is expected from the (111)-orientation of the CSO crystal. Naively, a cubic magnetocrystalline anisotropy in the Py layer could explain the observation.<sup>40</sup> Yet, it is not clear why such a crystalline structure should have developed when considering either the (111)-oriented substrate or the continuous rotation of the sample during the deposition process.

The chiral magnet/ferromagnet heterostructure proves to be a highly complex material system raising further questions about anisotropic interaction parameters and fundamental symmetry manifestations that go beyond the scope of this work. To phenomenologically model the data in Figs. 4(a) and 4(b), we use a Landau–Lifshitz–Gilbert (LLG) approach, where we treat the magnetization dynamics in the sample as a three-layer system consisting of the uncoupled Py and CSO layer as well as an interfacial layer as shown at the top of Fig. 2(b). Here, introducing an interfacial layer that inherits properties from Py and CSO layers effectively captures the coupling between the two and phenomenologically models a new mode that becomes active in this bilayer. Thereby, the magnetization dynamics of each of these three layers are treated as macrospins. In our model, we treat CSO as a ferromagnet, as it has been demonstrated that ferrimagnets can be modeled as ferromagnets when considering dynamics in the GHz regime.<sup>41,42</sup> The equation of motion for magnetization  $\mathbf{M}_i$  then reads

$$\frac{d\mathbf{M}_i}{dt} = -\gamma_i \mathbf{M}_i \times \mu_0 \mathbf{H}_{\text{eff}_i}(\phi_H) + \frac{\alpha_i}{M_{s_i}} \mathbf{M}_i \times \frac{d\mathbf{M}_i}{dt}. \quad (1)$$

Here,  $\gamma_i$  is the gyromagnetic ratio and  $\alpha_i$  is the Gilbert damping parameter of layer  $i$ . For all three magnetic layers, the effective field  $\mathbf{H}_{\text{eff}_i}$

accounts for the external field, the driving field, and the demagnetization field. The effective magnetic field  $\mathbf{H}_{\text{eff}_{\text{CSO}}}$  of the CSO is, thus, given by

$$\mathbf{H}_{\text{eff}_{\text{CSO}}}(\phi_H, t) = \mu_0 \mathbf{H}_{\text{ext}} \hat{\mathbf{x}} - \mu_0 \begin{pmatrix} N_x(\phi_H) \cdot M_s \\ N_y(\phi_H) \cdot m_{y_i}(t) \\ N_z \cdot m_{z_i}(t) \end{pmatrix}. \quad (2)$$

The angle dependent demagnetization factors  $N_x(\phi_H)$ ,  $N_y(\phi_H)$ , and  $N_z$  as well as the ansatz for the dynamic magnetization  $\mathbf{m}_i(t)$  are given in [supplementary material S7](#). In the case of the Py layer,  $\mathbf{H}_{\text{eff}_{\text{Py}}}$  additionally includes a phenomenological uniaxial magnetic anisotropy field  $\mathbf{B}_u$ , which is expected due to the demagnetization fields of the CSO and can be regarded effectively as a shape anisotropy of the CSO. However, a finite contribution due to the trapped flux in the superconducting coils is also to be expected (see [supplementary material S6](#)). Furthermore, it includes a phenomenological cubic anisotropy field  $\mathbf{B}_c$  that we assume to exist at the interface to explain the data. We note, again, that the fourfold symmetry does not correspond to the cubic anisotropy of CSO, because the projection of the cubic anisotropy to the (111) plane would result in a threefold symmetry

$$\mathbf{H}_{\text{eff}_{\text{Py}}}(\phi_H, t) = (\mu_0 \mathbf{H}_{\text{ext}} + \mathbf{B}_u \sin(\phi_H)^2 + \mathbf{B}_c \sin(2\phi_H)^2) \hat{\mathbf{x}} - \mu_0 m_{z_i}(t) \hat{\mathbf{z}}. \quad (3)$$

The effective magnetic field  $\mathbf{H}_{\text{eff}_{\text{HM}}}$  of the HM as well additionally accounts for a phenomenological cubic anisotropy field  $\mathbf{B}_c$

$$\mathbf{H}_{\text{eff}_{\text{HM}}}(\phi_H, t) = (\mu_0 \mathbf{H}_{\text{ext}} + \mathbf{B}_c \sin(2\phi_H)^2) \hat{\mathbf{x}} - \mu_0 m_{z_i}(t) \hat{\mathbf{z}}. \quad (4)$$

In Figs. 4(a) and 4(b), the Py (blue line), HM (orange line), and CSO (green line) resonance frequencies simulated with Eq. (1) are in good agreement with the measurement data (symbols).

In conclusion, we investigated the coupled magnetization dynamics in a CSO/Py heterostructure by broadband ferromagnetic resonance experiments at cryogenic temperatures. We found that a hybrid mode at the CSO/Py interface is excited. While a microscopic picture for the formation of the HM is so far missing, our experimental findings pave the way for future experiments on coupled spin dynamics in topologically non-trivial magnetic bilayer systems, which have recently attracted great interest from the viewpoint of possible applications in high-performance memory devices.<sup>7,32,43</sup>

See the [supplementary material](#) for additional measurements of the CSO/Py heterostructure and detailed information on the fitting and simulation methods.

We gratefully acknowledge the financial support by the Deutsche Forschungsgemeinschaft (DFG, German Research Foundation) via Nos. WE 5386/5-1 and BA 2181/19-1 and financial support from the Spanish Ministry for Science and Innovation—AEI Grant No. CEX2018-000805-M (through the “Maria de Maeztu” Programme for Units of Excellence in R&D). We would also like to thank M. Müller for support in carrying out some of the measurements.

## AUTHOR DECLARATIONS

### Conflict of Interest

The authors have no conflicts to disclose.

## Author Contributions

Carolina Lüthi and Luis Flacke contributed equally to this work.

**Carolina Lüthi:** Data curation (equal); Formal analysis (equal); Writing – original draft (equal). **Luis Flacke:** Data curation (equal); Formal analysis (equal); Writing – original draft (equal). **Aisha Aqeel:** Resources (lead). **Akashdeep Kamra:** Formal analysis (equal); Writing – review & editing (equal). **Rudolf Gross:** Writing – review & editing (equal). **Christian Back:** Formal analysis (equal); Writing – review & editing (equal). **Mathias Weiler:** Conceptualization (equal); Formal analysis (equal); Supervision (equal); Writing – review & editing (equal).

## DATA AVAILABILITY

The data that support the findings of this study are available from the corresponding author upon reasonable request.

## REFERENCES

1. Stasinopoulos, S. Weichselbaumer, A. Bauer, J. Waizner, H. Berger, M. Garst, C. Pfeleiderer, and D. Grundler, *Sci. Rep.* **7**, 7037 (2017).
2. C. Back, V. Cros, H. Ebert, K. Everschor-Sitte, A. Fert, M. Garst, T. Ma, S. Mankovsky, T. L. Monchesky, M. Mostovoy, N. Nagaosa, S. S. P. Parkin, C. Pfeleiderer, N. Reyren, A. Rosch, Y. Taguchi, Y. Tokura, K. von Bergmann, and J. Zang, *J. Phys. D* **53**, 363001 (2020).
3. D. Okuyama, M. Bleuel, J. S. White, Q. Ye, J. Krzywon, G. Nagy, Z. Q. Im, I. Živković, M. Bartkowiak, H. M. Rønnow, S. Hoshino, J. Iwasaki, N. Nagaosa, A. Kikkawa, Y. Taguchi, Y. Tokura, D. Higashi, J. D. Reim, Y. Nambu, and T. J. Sato, *Commun. Phys.* **2**, 79 (2019).
4. W. Legrand, D. Maccariello, N. Reyren, K. Garcia, C. Moutafis, C. Moreau-Luchaire, S. Collin, K. Bouzehouane, V. Cros, and A. Fert, *Nano Lett.* **17**, 2703 (2017).
5. S. Woo, K. Litzius, B. Krüger, M.-Y. Im, L. Caretta, K. Richter, M. Mann, A. Krone, R. M. Reeve, M. Weigand, P. Agrawal, I. Lemesch, M.-A. Mawass, P. Fischer, M. Kläui, and G. S. D. Beach, *Nat. Mater.* **15**, 501 (2016).
6. W. Jiang, P. Upadhyaya, W. Zhang, G. Yu, M. B. Jungfleisch, F. Y. Fradin, J. E. Pearson, Y. Tserkovnyak, K. L. Wang, O. Heinonen, S. G. E. te Velthuis, and A. Hoffmann, *Science* **349**, 283 (2015).
7. A. Fert, V. Cros, and J. Sampaio, *Nat. Nanotechnol.* **8**, 152 (2013).
8. J. Sampaio, V. Cros, S. Rohart, A. Thiaville, and A. Fert, *Nat. Nanotechnol.* **8**, 839 (2013).
9. F. Jonietz, S. Mühlbauer, C. Pfeleiderer, A. Neubauer, W. Munzer, A. Bauer, T. Adams, R. Georgii, P. Boni, R. A. Duine, K. Everschor, M. Garst, and A. Rosch, *Science* **330**, 1648 (2010).
10. X. Z. Yu, N. Kanazawa, W. Z. Zhang, T. Nagai, T. Hara, K. Kimoto, Y. Matsui, Y. Onose, and Y. Tokura, *Nat. Commun.* **3**, 988 (2012).
11. X. Z. Yu, Y. Onose, N. Kanazawa, J. H. Park, J. H. Han, Y. Matsui, N. Nagaosa, and Y. Tokura, *Nature* **465**, 901 (2010).
12. S. Mühlbauer, B. Binz, F. Jonietz, C. Pfeleiderer, A. Rosch, A. Neubauer, R. Georgii, and P. Boni, *Science* **323**, 915 (2009).
13. T. Schwarze, J. Waizner, M. Garst, A. Bauer, I. Stasinopoulos, H. Berger, C. Pfeleiderer, and D. Grundler, *Nat. Mater.* **14**, 478 (2015).
14. A. Chacon, L. Heinen, M. Halder, A. Bauer, W. Simeth, S. Mühlbauer, H. Berger, M. Garst, A. Rosch, and C. Pfeleiderer, *Nat. Phys.* **14**, 936 (2018).
15. A. Aqeel, J. Sahliger, T. Taniguchi, S. Mändl, D. Mettus, H. Berger, A. Bauer, M. Garst, C. Pfeleiderer, and C. H. Back, *Phys. Rev. Lett.* **126**, 017202 (2021).
16. I. Stasinopoulos, S. Weichselbaumer, A. Bauer, J. Waizner, H. Berger, S. Maendl, M. Garst, C. Pfeleiderer, and D. Grundler, *Appl. Phys. Lett.* **111**, 032408 (2017).
17. M. Weiler, A. Aqeel, M. Mostovoy, A. Leonov, S. Geprägs, R. Gross, H. Huebl, T. T. M. Palstra, and S. T. B. Goennenwein, *Phys. Rev. Lett.* **119**, 237204 (2017).
18. L. Liensberger, F. X. Haslbeck, A. Bauer, H. Berger, R. Gross, H. Huebl, C. Pfeleiderer, and M. Weiler, *Phys. Rev. B* **104**, L100415 (2021).
19. S. Seki, M. Garst, J. Waizner, R. Takagi, N. D. Khanh, Y. Okamura, K. Kondou, F. Kagawa, Y. Otani, and Y. Tokura, *Nat. Commun.* **11**, 256 (2020).
20. P. Bruno, *Phys. Rev. B* **52**, 411 (1995).
21. D. C. Crew, J. Kim, K. Barmak, and L. H. Lewis, *J. Appl. Phys.* **93**, 7235 (2003).
22. D. E. Gonzalez-Chavez, R. Dutra, W. O. Rosa, T. L. Marcondes, A. Mello, and R. L. Sommer, *Phys. Rev. B* **88**, 104431 (2013).
23. B. Heinrich, Y. Tserkovnyak, G. Woltersdorf, A. Brataas, R. Urban, and G. E. W. Bauer, *Phys. Rev. Lett.* **90**, 187601 (2003).
24. R. D. McMichael, M. D. Stiles, P. J. Chen, and W. F. Egelhoff, *J. Appl. Phys.* **83**, 7037 (1998).
25. S. Schäfer, N. Pachauri, C. K. A. Mewes, T. Mewes, C. Kaiser, Q. Leng, and M. Pakala, *Appl. Phys. Lett.* **100**, 032402 (2012).
26. G. Woltersdorf, O. Mosendz, B. Heinrich, and C. H. Back, *Phys. Rev. Lett.* **99**, 246603 (2007).
27. M. Julliere, *Phys. Lett. A* **54**, 225 (1975).
28. M. N. Baibich, J. B. Broto, A. Fert, F. van Nguyen Dau, F. Petroff, P. Etienne, G. Creuzet, A. Friederich, and J. Chazelas, *Phys. Rev. Lett.* **61**, 2472 (1988).
29. G. Binasc, P. Grünberg, F. Saurenbach, and W. Zinn, *Phys. Rev. B* **39**, 4828 (1989).
30. S. Klingler, V. Amin, S. Geprägs, K. Ganzhorn, H. Maier-Flaig, M. Althammer, H. Huebl, R. Gross, R. D. McMichael, M. D. Stiles, S. T. B. Goennenwein, and M. Weiler, *Phys. Rev. Lett.* **120**, 127201 (2018).
31. F. Hellman, A. Hoffmann, Y. Tserkovnyak, G. S. D. Beach, E. E. Fullerton, C. Leighton, A. H. MacDonald, D. C. Ralph, D. A. Arena, H. A. Dürr, P. Fischer, J. Grollier, J. P. Heremans, T. Jungwirth, A. V. Kimel, B. Koopmans, I. N. Krivorotov, S. J. May, A. K. Petford-Long, J. M. Rondinelli, N. Samarth, I. K. Schuller, A. N. Slavin, M. D. Stiles, O. Tchernyshyov, A. Thiaville, and B. L. Zink, *Rev. Mod. Phys.* **89**, 025006 (2017).
32. A. Takeuchi, S. Mizushima, and M. Mochizuki, *Sci. Rep.* **9**, 9528 (2019).
33. Y. Kawaguchi, Y. Tanaka, and N. Nagaosa, *Phys. Rev. B* **93**, 064416 (2016).
34. F. Qian, H. Wilhelm, A. Aqeel, T. T. M. Palstra, A. J. E. Lefering, E. H. Brück, and C. Pappas, *Phys. Rev. B* **94**, 064418 (2016).
35. A. Aqeel, J. Sahliger, G. Li, J. Baas, G. R. Blake, T. T. M. Palstra, and C. H. Back, *Phys. Status Solidi B* **259**, 2100152 (2022).
36. H. Maier-Flaig, S. T. B. Goennenwein, R. Ohshima, M. Shiraishi, R. Gross, H. Huebl, and M. Weiler, *Rev. Sci. Instrum.* **89**, 076101 (2018).
37. R. Engel-Herbert and T. Hesjedal, *J. Appl. Phys.* **97**, 074504 (2005).
38. M. Garst, J. Waizner, and D. Grundler, *J. Phys. D* **50**, 293002 (2017).
39. A. Kamra and W. Belzig, *Phys. Rev. B* **94**, 014419 (2016).
40. L. Liensberger, A. Kamra, H. Maier-Flaig, S. Geprägs, A. Erb, S. T. B. Goennenwein, R. Gross, W. Belzig, H. Huebl, and M. Weiler, *Phys. Rev. Lett.* **123**, 117204 (2019).
41. A. J. Princep, R. A. Ewings, S. Ward, S. Tóth, C. Dubs, D. Prabhakaran, and A. T. Boothroyd, *npj Quantum Mater.* **2**, 63 (2017).
42. Y. Luo, G. G. Marcus, B. A. Trump, J. Kindervater, M. B. Stone, J. A. Rodriguez-Rivera, Y. Qiu, T. M. McQueen, O. Tchernyshyov, and C. Broholm, *Phys. Rev. B* **101**, 144411 (2020).
43. A. Soumyanarayanan, N. Reyren, A. Fert, and C. Panagopoulos, *Nature* **539**, 509 (2016).